

Pressure and temperature dependence of the electric modulus and loss factor of Poly(vinyl alcohol)/Poly(vinylidene fluoride) blends reinforced with Nano - Graphene platelets

Eirini Kolonelou^a, Eirini Loupou^a, Elias Sakellis^{a,b}, Anthony N. Papathanassiou^{a,*}

^a National and Kapodistrian University of Athens, Physics Department, Panepistimioupolis, GR 15784, Zografos, Athens, Greece

^b National Center of Natural Sciences Demokritos, Institute of Nanomaterials and Nanotechnology, Aghia Paraskevi, Athens, Greece

ARTICLE INFO

Keywords:

Polyvinyl alcohol
Polyvinylidene fluoride
Electron-conducting polymers
Graphene
Nanocomposites
Piezoelectricity
Broadband dielectric spectroscopy

ABSTRACT

Poly(vinyl alcohol)/Poly(vinylidene fluoride) blends reinforced with Nano - Graphene Platelets render piezoelectric by combining uniaxial plastic deformation and polarization. Comparative Broadband Dielectric Spectroscopy on fresh and piezoelectric specimens were carried out at various temperature and hydrostatic pressure states. Dc conductivity, which results from inter-NGP fluctuation induced tunneling of electrons through the effective potential barrier set by the polymer, involves two charge transfer mechanisms. The shift of the glass transition temperature and the temperature triggering a kinetic process due to the enhancement of the mobility of water molecules bound to PVA, upon pressure are detected indirectly through associated changes to the conductivity modes. NGP filling induces a couple of interfacial charge trapping. Relaxations exhibit different thermodynamics and different dependencies for fresh and piezoelectric specimens on pressure. Hydrostatic compression of heterogeneous matter results in an inhomogeneous internal stress field, whereas stress is locally amplified. In PNC, small scale relaxation is disturbed by the spatial fluctuation of the internal stress field. Rendering the PVDF grains piezoelectric, local stress amplification induces fluctuations of the local electric field. Fluctuations (of the internal stress or electric field) affect rather a short-range charge relaxation, rather than macroscopic dc conductivity.

1. Introduction

Poly(vinylidene fluoride) (PVDF) is a widely used semicrystalline polymer with good mechanical properties, resistance to chemicals, high dielectric permittivity and exceptional pyro- and piezoelectric properties [1,2]. Amongst other uses, materials of piezoelectric PVDF are of great interest in broadband acoustic and ultrasonic transducers [3], particularly for medical imaging applications since they are flexible and with acoustic impedance similar to water and biological tissues [4]. It is well known that quantitative modeling of the frequency response of piezoelectric transducers requires the accurate characterization of the material properties [5]. Compared to inorganic piezoelectric materials, the internal losses (both mechanical and electrical) are much larger in polymers. In consequence, it is very important to consider the frequency, pressure and temperature dependence of the relative complex dielectric permittivity ϵ^* , when describing transducers based on piezoelectric polymers. XRD, FTIR and Raman spectroscopy on Poly(vinyl alcohol)

PVA)/poly (vinylidene fluoride) (PVDF) blends of variable mass ratios indicated that optimal structural and thermal stability and properties are attained at concentration 22.5 wt % PVDF [6] (see Table 1).

The addition of graphene nanoparticles to PVA improves the composite's electrical conductivity and thermal stability. NGPs (nano-graphene platelets) are a cost-effective way to strengthen a polymer. The electrical conductivity of the composite can be comparable to that of a semiconductor at mass fractions low enough to avoid a continuous percolation network due to physical touching among NGPs. Percolation thresholds have been found in polymer nano-composites (PNCs) loaded with diverse carbon allotropes [7,8] at very low mass fractions. Inter-NGP tunneling occurs through the separating polymer barrier due to thermal changes in the Fermi level of electron states in NGPs. The electron percolation network consists of isolated NGPs (or isolated aggregates) and the inter-NGP polymer regions through which the inter-NGP tunneling current flows; the former consists of isolated NGPs (or isolated aggregates) and the inter-NGP polymer regions through

* Corresponding author.

E-mail address: antpapa@phys.uoa.gr (A.N. Papathanassiou).

<https://doi.org/10.1016/j.jpcs.2023.111277>

Received 27 June 2022; Received in revised form 9 February 2023; Accepted 11 February 2023

Available online 1 March 2023

0022-3697/© 2023 Elsevier Ltd. All rights reserved.

Table 1

Description and code naming of the materials studied in the present work.

sample description	code name
PVA/PVdF at mass ratio 2:1 (unfilled matrix)	Matrix
Nanocomposite with 2% NGP	PNC
Nanocomposite with 2% NGP + Piezo-electric	PNC-PZ

which the inter-NGP tunneling current flows. The tunneling current is determined by the tunneling volume or inter-NGP distance, as well as the polymer matrix's polarizability and thermodynamic state (glassy, semi-crystalline or rubber). Pressure sensing or pressure electro-switching PNCs can be developed by tweaking the pressure dependence of these parameters. As a result, it's critical to identify specific electric charge flow pathways and link them to heterogeneity, the polymer's glassy or rubber state, and any kinetic phenomena that may occur, such as solvent water molecule movement. Pressure-induced electro-switching has been seen in PVA/NGP composites as a result of competition between the components outlined above [8]. It is worth noticing that the piezoelectric nature of PVdF in PVdF/PVA compounds loaded with graphene nanostructures have proved to be important for bio-medicine: The osteogenesis rate of human-induced pluripotent stem cells (hiPSCs) cultured on PVdF-PVA-graphene oxide (GO) electro spun scaffolds is significantly higher than other scaffolds, making them a highly promising scaffold-stem cell system for bone remodeling medicine [9].

The nanocomposite material in the present work consists of a PVA/PVdF blend at a mass ratio 3:1, obtained by drop casting a water solution of α -PVA and suspended PVdF micro-grains, reinforced with 2 wt % dispersed NGPs. The as-received fresh polymer nanocomposite (PNC) renders to piezoelectric (PNC-PZ) by applying mechanical stress and electric field to the PNC. Differential Scanning Calorimetry (DSC), Broadband Dielectric Spectroscopy (BDS), electro-mechanical coupling response (EMCR) and Scanning Electron Microscopy (SEM) studies at ambient pressure and different temperatures on PNC and PNC-PZ provided information about the thermal and electric properties at ambient pressure conditions: Two dc conductivity mechanisms appear in successive temperature regions. Their temperature dependencies obey the fluctuation induced tunneling (FIT) of electrons among neighboring NGPs separated by the polymer matrix. The bounds of the aforementioned temperature regions coincide with structural phase transitions in the polymer blend and the onset of a kinetic process related with the enhancement of the mobility of water molecules bound to PVA. A couple of dielectric relaxation mechanisms are correlated with the NGP inclusions. The temperature dependencies of the frequencies of maximum loss angle indicate that relaxation occurs by FIT of electrons, too. Fresh specimens render piezoelectric, by applying uniaxial stress and electric polarization. While the mass fraction of piezoelectric PVdF grains is only 25%, the overall electromechanical coefficient comparable to neat piezoelectric PVdF. BDS and DSC experiments on piezoelectric composites converge to the conclusion that the electro-activity of PVdF grains affects weakly the electric and thermal properties of the nanocomposites [6].

In the present work, were employing BDS on PNC and PNC-PZ at combined pressure and temperature states ranging from ambient pressure to 1750 bar and from 293 K 393 K, respectively. The application of hydrostatic pressure affects the structure and the electrical properties of the nanocomposite in different ways, such as:

- (i) The distance between neighboring NGPs gets reduced and, hence, the inter-NGP tunneling length.
- (ii) The polarizability of the polymer blend separating NGPs reduces and the inter-NGP tunneling current weakens.
- (iii) The glass transition temperature changes monotonically with pressure; therefore, dc conductivity mechanisms are tuned by the

modification of the polymer blend matrix from a rubber to a glassy state.

- (iv) Heterogeneity is likely to change due to small scale re-ordering of their elements, so as to make better use of the volume of the compressed material.
- (v) The heterogeneous structure of the material and the dispersion of hard sharp NGP flakes, induce local fluctuations of the internal stress field when the sample is externally hydrostatically compressed. Additionally, if one of the constituents of the blend is piezoelectric, amplified local stress fields may induce fluctuations in the local electric fields.

The role of the above-mentioned phenomena on the electric and dielectric properties of PVA/PVdF blends loaded with NGPs is explored in the present work. The functionality of the materials studied in the present work as flexible, non-toxic paintable pressure sensors and energy harvesters of spare vibrational energy, depends on the synergy of different microscopic processes. The knowledge of how each one of these depends on pressure and temperature determine at which environmental conditions, the material's efficiency is optimal and which parameters should furthermore be tailored to improve functionality.

2. Materials and methods

The starting materials used for the preparation of the free-standing bulk specimens comprised polyvinyl alcohol (PVA), (C₂H₄O)_n, purity 99,5%; ASG SCIENTIFIC, CAS 9002-89-5), powder of poly(vinylidene fluoride) (PVdF) of molecular weight 534.000 (Sigma Aldrich Ltd) CAS 24937-79-9) of mean grain size 2.5 μ m [10] and graphene nano-platelets (NGPs) (Angstrom Materials Ltd) which were used without any further purification. According to the manufacturer, the lateral size of NGPs is $\leq 10 \mu$ m² and the average through dimensions were 50–100 nm determined by BET surface analysis and size distribution. Earlier publications on water soluble polymers (such as PVA, PVP and blends) reinforced with different mass fractions of NGPs by solution casting similar to that mentioned in the present work, indicated that the critical mass fraction of NGPs ranges from 0.1 to 0.3 % wt. % [7,8,11]; the conductivity percolation cluster is formed at much lower fraction than that required for the formation of a continuous physical NGPs, due to the inter-NGP tunneling current through the polymer barrier. Here, the mass fraction is 2 wt %, i.e., at a value close enough and above percolation threshold, but, low enough to prevent the formation of a continuous network of NGPs. The homogeneous distribution of NGPs and the absence of any continuous network of NGPs were verified by SEM inspection [6]. In a past work, we have used NGP composites in PVA blended with 25 wt % α -poly (vinylidene fluoride) (PVdF) micro-grains. The structural and thermal stability of PVA/PVdF blends, the way that the composite becomes piezoelectric, after mechanical stressing and polarization, were published recently [6]. SEM, DSC, electromechanical coupling characterization and BDS at ambient pressure and various temperatures on PNC and PNC-PZ are reported on [6], too.

The percolation threshold (0.1–0.3 wt %, at ambient conditions) changes on pressure: to a first approximation, hydrostatic compression yields a reduction of the volume of the specimen and, subsequently, an increase of the volume fraction of the conductive inclusions. In the present work, we require a percolation cluster being created, so as to study how the inter-NGP tunneling volume is affected at various pressures (and temperatures): 2 wt % NGP filler ensures that the our materials are electrically percolative, beyond its criticality (0.1–0.3 wt %) and unaffected from pressure and temperature induced fluctuations of the percolation threshold.

3. Theoretical background

The increase of the mass fraction of nano-graphene platelets (NGPs) results a systematic increase of the dc conductivity of the nano-

composite blends [7]. The overall dc conductivity is therefore tuned by the electronic density dictated by the free electrons available by NGPs. A mass fraction of 2 wt % in nano-graphene platelets provide a high electron density distributed in conductive islands within the polymer matrix. The values of the effective activation energy are of the order of a few meV, i.e., orders of magnitude smaller than the band gap of an insulator (polymer). Small mass electrons, rather than ions, can perform inter-NGP quantum mechanical tunneling (expensing a few meV energy) through the polymer separation. In the manuscript, we state that electron transport dominates: i.e., any ionic transport operating in parallel with electron conduction, is weak compared with the avalanche of electrons.

Sheng proposed the Fluctuation Induced Tunneling (FIT) theory to explain electronic transport in heterogeneous materials with an insulating matrix and distributed conducting inclusions [12]. FIT initially explained electronic transport in granular metals, with thermal fluctuations of the Fermi energy level assisting inter-grain tunneling of electrons over a separating insulating barrier. It has also been effectively used to a wide range of electron-conducting in homogeneously disordered materials, including conducting polymers and composites. As a result, the temperature dependency of dc conductivity σ_{dc} is as follows:

$$\sigma_{dc} = \sigma_0 \exp\left(\frac{-T_1}{T + T_0}\right) \quad (1)$$

Sheng and Klafter [13,14] demonstrated that the latter function is $T^{-1/2}$ dependent:

$$\sigma_{dc} = \sigma'_0 \exp\left(\frac{T_1}{T}\right)^{1/2} \quad (2)$$

Both (macroscopic) dc conductivity and localized charge mobility are caused by a certain sort of atomic charge flow event. If Γ_{ij} denotes the transition rate of electric charges tunneling from site i to site j , under the influence of an external field, then, $\sigma_{dc} \propto \Gamma_{ij}$ and $\tau^{-1} \propto \Gamma_{ij}$, where τ is the dielectric relaxation time. In the frequency domain, dielectric loss maximizes at $f_{max} = 1/\tau$, which implies that $f_{max} \propto \Gamma_{ij}$. As a result, the temperature dependence of the relaxation maxima resembles that of σ_{dc} , i.e.:

$$f_{max} \propto \exp\left(\frac{-T_1}{T + T_0}\right) \quad (3)$$

and, approximately:

$$f_{max} \propto \exp\left(\frac{T_1}{T}\right)^{1/2} \quad (4)$$

The height of the effective potential barrier involved in FIT, within the assumptions and the approximations made to derive eq. (4), is of the order of magnitude $k_B T_1$, where k_B denotes the Boltzmann's constant. Approximate $T^{-1/2}$ dependence resemble that of the Mott's Variable Range Hopping (VRH), but has different physical basis: in brief, FIT accounts for in-homogeneous disordered materials whereas electron states extended over the volume of each one conducting grain and tunnel to neighboring grains due to thermal fluctuations of the Fermi level, while VRH accounts for phonon assisted tunneling of electrons from a localized state to another one within a homogeneously disordered solid.

4. Results and discussion

4.1. Dc conductivity study by means of complex electric modulus $M^*(f)$ studies

Bypass of undesirable electrode polarization effects in the determination of the dc conductivity σ_{dc} is achieved through the use complex electric modulus function: $M^* = \frac{1}{\epsilon^*} = M' + iM''$, where:

$$M'(f) = M_s \frac{(f\tau_\sigma)^2}{1 + (f\tau_\sigma)^2} \quad (5)$$

$$M''(f) = M_s \frac{f\tau_\sigma}{1 + (f\tau_\sigma)^2} \quad (6)$$

A low frequency "conductivity peak," which originates from the dc component alone, builds up a plot of $M(f)$, reaching a maximum at $f_{max,\sigma} = (2\pi\tau_\sigma)^{-1}$, or:

$$f_{max,\sigma} = \sigma_{dc} / (2\pi\epsilon_0\epsilon_\infty) \quad (7)$$

where $\epsilon_\infty \equiv \epsilon'(f \rightarrow \infty)$. The fact that $\epsilon'(f \rightarrow \infty)$ has a mild temperature dependence is widely assumed (and confirmed by our experimental findings). As a result, the FIT equation (3) and its approximation (eq. (4)) can be utilized to examine the $f_{max,\sigma}(T)$ data. Dielectric relaxations are recorded as well, but the maxima are shifted to a higher frequency than those seen in $\epsilon''(f)$ or $\tan\delta(f)$ [14,15]. $M(f)$ is a step-like plot, and its high frequency plateau yields $M_s \equiv M'(f \rightarrow \infty)$ as well as the (relative) static dielectric constant $\epsilon_s = \frac{1}{M_s}$. By definition, the electric modulus function suppresses the unwanted low frequency space charge capacitance contributions, allowing a precise estimate of both dc conductivity and the static dielectric constant ϵ_s (see Fig. 8).

In Fig. 9, where isotherms of $M''(f)$ at different pressures are depicted for PNC and PNC-PZ, a low-frequency conductivity peak dominates. In all the plots, the shift of peaks to higher frequency upon temperature indicates that the relaxation time becomes shorter. It is worth to notice that the undesirable electrode polarization effects dominating at low frequencies, contribute to the low frequency tail of a conductivity peak, leaving unaffected the position and value of the peak maximum [16]. Hence, by simply using the electric modulus function we have a clear (free from electrode polarization) insight to the dc conductivity itself [17].

The temperature history of dc is traced from the shift of the conductivity peak towards higher frequencies with increasing temperature (Fig. 4), as discussed previously. To see if one or more dc conductivity mechanisms work over the temperature range spanned by BDS tests, we looked at whether $\log f_{max,\sigma}(T^{-1/2})$ has one or more linear portions each corresponding to a separate FIT mechanism specified by eq (2). Indeed, the data points in Fig. 3 are distributed over two linear zones, each of which corresponds to a different dc conductivity mode: C1 and C2. As the temperature rises, the switch of the dc conductivity mechanism C1 to C2 marks a shift in the temperature dependence and corresponds to the commencement of the kinetic process (attributed to increased water molecule mobility) shown in the first scan of the DSC thermograms. Dc electron conduction by FIT across the whole volume of the specimen captures heat changes in the polymer matrix [6].

4.1.1. Estimation of the pressure dependence of the glass transition temperature $T_g(P)$ from electric modulus studies

In Fig. 1, $\log f_{max,\sigma}(T)$ at different pressures are depicted. At ambient pressure, two successive FIT dc conductivity mechanisms (labeled as C1 and C2, respectively) are detected [6]. The glass transition temperature for PNC and PNC-PZ was found by DSC at 20 °C and 27 °C, respectively [6]. In the ambient pressure diagram of Fig. 1, the vertical arrow points toward the temperature range T_g were found by DSC. We stress that DSC is a non-equilibrium method and the resulting T values depends, more or less, on the scan rate; nevertheless, it is worthy to highlight in Fig. 1 the temperature region where the values of T_g were detected (by a vertical full arrow); the open arrow point the temperature around which a kinetic process of water molecules bound to PVA were detected by DSC [6]. On increasing pressure, we observe that the temperature range whereas a thermally activated FIT applies is gradually restricted within a high temperature region. The transition temperature from a weak to stronger temperature dependence, initiates from the T_g

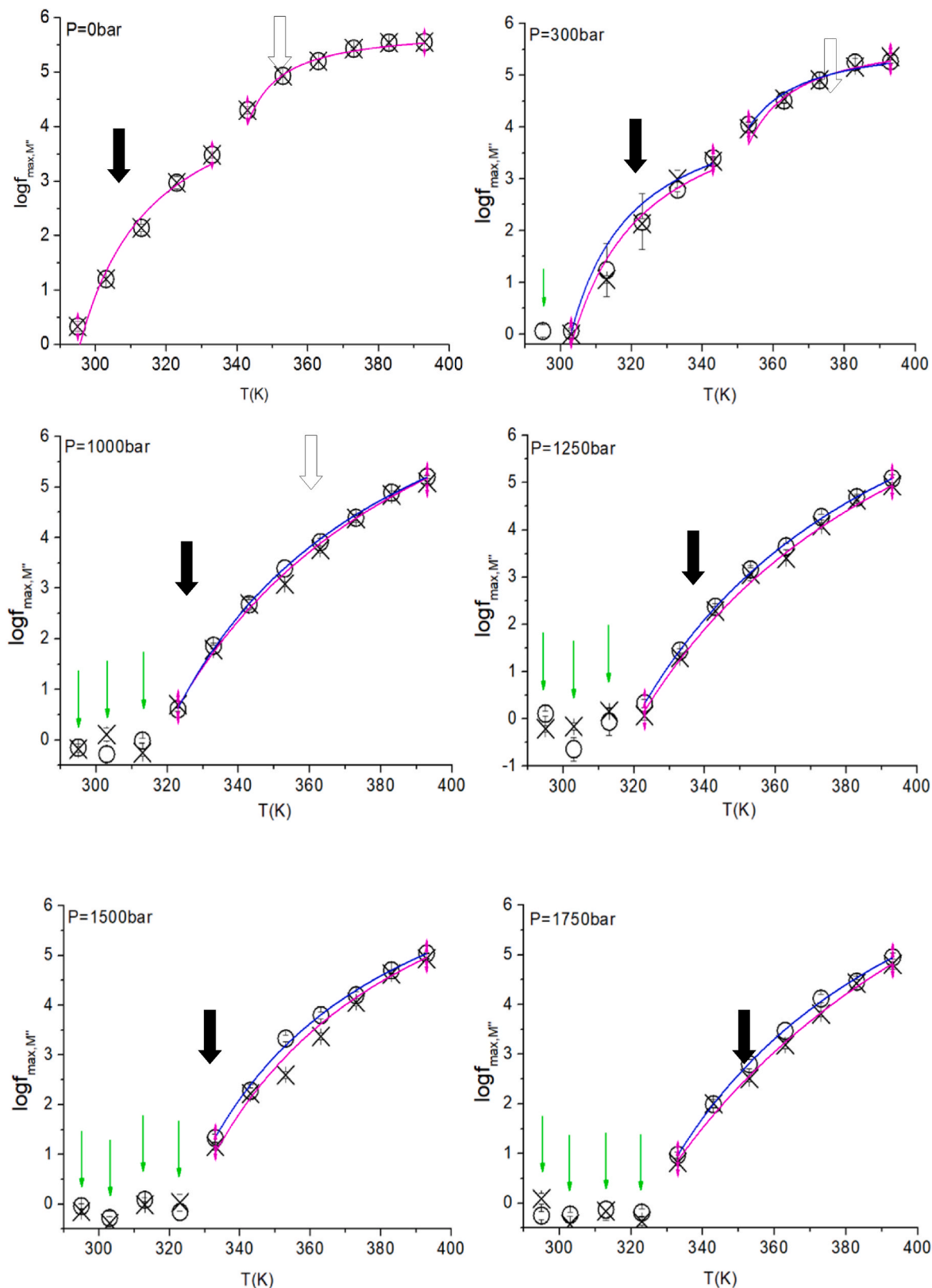


Fig. 1. Isobaric diagrams of $\log f_{\max, M''}(T)$ data points for PNC (o) and PNC-PZ (\times). The **full** arrows at the ambient pressure diagram, indicates the glass transition temperature T_g determined by DSC (20 °C for PNC and 27 °C for PNC-PZ) and [6]; the **open** arrow point the temperature around which a kinetic process of water molecules bound to PVA were detected by DSC [6]. On increasing pressure, it indicates the transition temperature from a weak to stronger thermally activated behavior and signatures the glass transition temperature, hence, providing the rate: $\frac{dT_g}{dP} = 0.030(5) \frac{\text{grad}}{\text{bar}}$. Curves are regional best fits of the $T^{-1/2}$ FIT law (eq. (2)) to the data points.

value determined experimentally by DSC at ambient pressure and increases upon compression at a rate of $\frac{dT_g}{dP} = 0.030(5) \text{ grad/bar}$ and is attributed to the pressure coincides with the T_g determined by DSC and shift of the glass transition temperature. The latter is typically around $\frac{0.04 \text{ grad}}{\text{bar}}$ [18].

4.1.2. Effect of pressure on the activation energy $k_B T_1$ for dc conductivity

The temperature evolution of the maximum of the conductivity peak at ambient pressure was investigated thoroughly in Ref. [6]. Two dc conductivity mechanisms, labeled C1 and C2, each obeying a FIT law, operate in two successive temperature regions, respectively. Mechanism C2 is triggered above a temperature where a kinetic process initiates in DSC scans [6] and is attributed to an augmented mobility of water molecules bound to the hydrophilic PVA. The distinction among different conductivity mechanisms becomes difficult at elevated pressure, because of the shift of the glass transition temperature, the number of data points to be fitted above $T_g(P)$, reduces. The best visualization is achieved by plotting $\log f_{\max} M'' (T^{-1/2})$: according to eq. (2), straight lines are predicted for individual FIT mechanisms. In Fig. 2, a couple of $T^{-1/2}$ diagrams at 300 and 1750 bar, are comparatively shown. Above $T_g(P)$, conductivity mechanisms C1 and C2 appear as straight lines of different slopes. At 1750 bar, it is hard to detect and resolve different mechanisms; the data points above $T_g(P)$, lie on a single straight line.

Within the frame of the $T^{-1/2}$ dependent FIT model (eq. (2)), the activation energy (and a rough estimate of the related effective potential barrier) is about $k_B T_1$. The effective activation energies E_{C1} and E_{C2} , for the dc-conductivity mechanisms C1 and C2, respectively, as a function of pressure are presented in Fig. 3. Firstly, we observe that data points of both fresh PNC and PNC-PZ, that were rendered piezoelectric by axial deformation and polarization, share (within the experimental accuracy) a common trend upon pressure. Combined DSC and BDS experiments, at ambient pressure [6], indicated that a kinetic process due to enhanced activated mobility of water molecules bound to PVA, proceeds in parallel with conductivity mechanism C2. The activation energies for the dc conductivity mechanisms, which were resolved through the electric modulus function, are plotted against pressure in Fig. 3. Below 1000 bars, the data points distribute in two sets, each one attributed to the conduction mechanisms C1 and C2, respectively.

The activation volume for a thermally activated process is thermodynamically defined as: $v^{act} \equiv \left(\frac{\partial g^{act}}{\partial P} \right)_T$, where g^{act} denotes the Gibbs free energy per transition [8,19], which is, to a first approximation, roughly equal to the activation energy, we can write:

$$v^{act} \cong \left(\frac{\partial E}{\partial P} \right)_T \quad (8)$$

Therefore, v^{act} is a measure of the change of the effective potential

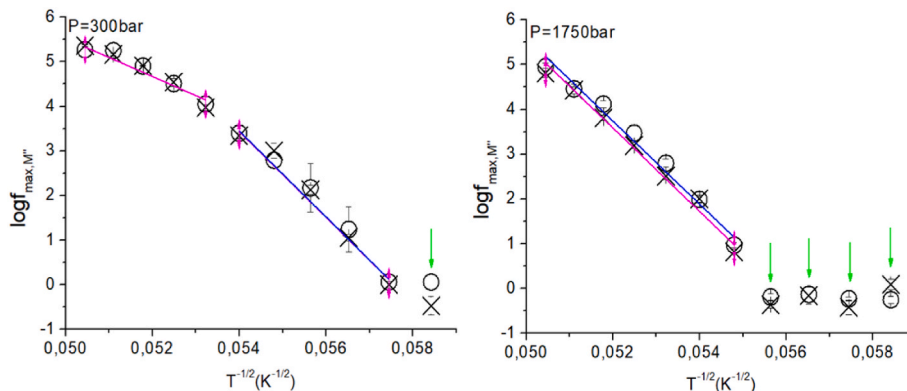


Fig. 2. $T^{-1/2}$ dependence of the conductivity relaxation peak observed in $M''(f)$. Linear regions signature individual dc conductivity mechanisms. Arrows indicate the data points corresponding to temperatures below $T_g(P)$, which depend weakly on temperature (o): PNC, (x): PNC-PZ.

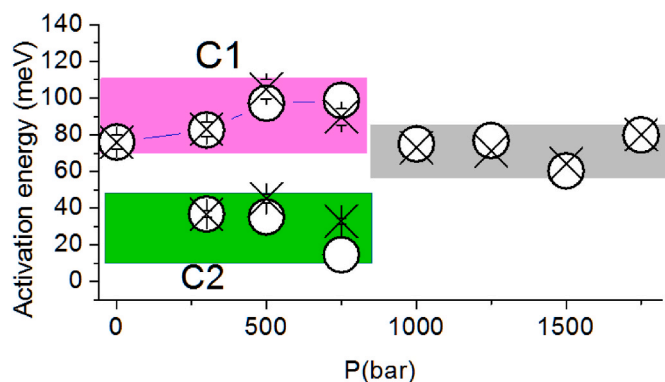


Fig. 3. The activation energy for dc conductivity as a function of pressure < Below 1000 bar, mechanisms C1 and C2 are detected. Above 1000 bar, a unique mechanism is detected. (o): PNC, (x): PNC-PZ.

barrier ($k_B T_1$ upon hydrostatic compression and its value can be positive, negative or null. The slope of straight line fitted to each one of the data points belonging to C1 and C2 (Fig. 3), equals (due to eq. (8)) the activation volume $v_{C1}^{act} = 4(2) \times 10^{-29} \text{ m}^3$ and $v_{C2}^{act} = 2(4) \times 10^{-29} \text{ m}^3$, respectively. Both values are too low (compared, for example, with typical values for ionic conductivity), evidencing that the overall dc conductivity to electron tunneling (FIT). This conclusion supports the attribution of the low activation energy values to electron tunneling.

Above 1000 bar, a single mechanism can be observed, which is interpreted as the result of the joint dependence of two thermal phenomena upon pressure:

- the glass transition temperatures measured at ambient pressure for PNC and PNC-PZ by DSC [6] move toward higher temperature.
- the kinetic process related to the increase of the mobility of water molecules bound to PVA, which was detected around 70 °C by DSC [6], is expected to shift toward higher temperature, as well.

In Fig. 3, we observe that the activation energy values of the single conductivity mechanism detected above 1000 bar, are laying between those of C1 and C2. It is more likely that a coupling of C1 and C2 occurs at high pressure, rather than identifying the high-pressure mechanism with C2.

4.2. Study of charge trapping through the tangent of the loss angle $\tan \delta(f)$

Study of dielectric relaxation phenomena is considered as a vital method to explore the molecular interaction in a polymer [20]. The

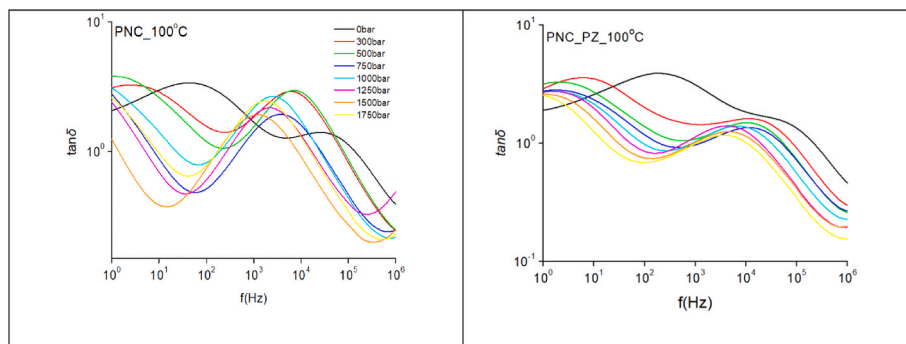


Fig. 4. $\tan\delta$ spectra at different pressures for PNC and PNC-PZ at 100 °C.

segmental motion of the polymer backbone within the polymer matrix plays an important role in ions transference that can be perceivable with the relaxation process [21]. Accordingly, to observe the relaxation behavior in the PNC films, the tangent loss ($\tan\delta$) was analyzed. The loss tangent ($\tan\delta$) can be defined as a ratio of dielectric loss per dielectric constant $\tan(\delta) = \frac{\epsilon''}{\epsilon'}$ (9) and it is a measure of electrical energy lost ratio to the stored energy in a periodic field [22,23].

In Fig. 1, isotherms of the dielectric loss factor $\tan\delta(f)$ of PNC and PNC-PZ at different pressures. At ambient pressure and 500 bar, the spectra consist of a couple of overlapping peaks, which shift toward higher frequencies on increasing temperature. We label DR1, $\tan\delta$ and DR2, $\tan\delta$ the longer and the shorter relaxation times mechanism, respectively. Their occurrence is related with the filling of the polymer blend by NGPs; they are attributed to inter-NGP tunneling restricted within localized territories of the PNC and polarization of individual NGP, respectively [6].

4.2.1. Effect of tuning $T_g(P)$ on the dielectric relaxation mechanisms

In Fig. 4, typical $\tan\delta(f)$ spectra, recorded at various pressure values and constant temperature are depicted, for PNC and PNC-PZ, respectively. Two overlapping relaxation mechanisms: the low and high frequency ones are labeled as DR1 and DR2, respectively. In fig. 8, $\tan\delta(f)$ isotherms for four different pressures sampled from the entire set of isobars recorded.

4.2.2. Relaxation activation energies within the FIT theory

In Fig. 5, some representative $\log_{\max, \tan\delta}(T^{-1/2})$ isobaric diagrams are presented. Each set of data points are fitted by a unique straight. Fitting eq. (4) to the $\log_{\max, \tan\delta}(T^{-1/2})$ data points the activation energy, which is roughly equal to the related effect potential barrier, can be estimated from the parameter magnitude T_1 of the FIT model (eq (3)) [13]: $E \approx k_B T_1$.

4.2.3. Pressure dependence of the relaxation activation energies

In Fig. 6, the relaxation activation energies for DR1 of PNC and PNC-PZ are plopped as a function of pressure. The corresponding data points exhibit a common increasing trend upon pressure. Moreover, there is not a clear and systematic discrimination between the data sets of PNC and PNC-PZ, respectively. We can, therefore, state that the capacitance mechanism related to DR1 is practically the same in fresh PNC and the uniaxially deformed and polarized specimens. The effective potential energy barrier for DR1 is not affected by the sample preparation history, i.e., the axial compression and polarization procedure to render fresh NPC piezoelectric. The large relaxation time of DR1 (compared to that of DR2) indicates localized relaxation involving multiple inter-NGP tunneling events. Consequently, DR1 proceeds within larger localization territories, in comparison with DR2.

A straight line was fitted to the data points of PNC and PNC-PZ, respectively (Fig. 6). The slope reveals the activation volume $v^{act} \cong \left(\frac{\partial E}{\partial P}\right)_T$ for each relaxation mechanism. The activation volume for DR1 is

$2.6(6) \times 10^{-29} \text{ m}^3$ for PNC and $2.9(5) \times 10^{-29} \text{ m}^3$ for PNC-PZ, respectively. In polar polymers with dispersed nano-carbons, the effect of hydrostatic compression on the inter-NGP tunneling through the potential barrier set by the polymer separation is dictated, to a first approximation, by two competing phenomena: the reduction of the tunneling length, which enhances the tunneling current and the reduction of the polarizability, which impedes tunneling. In PVA filled with NGPs around the percolation concentration threshold, we found that the role of the second phenomenon is quite important [8,19]. The latter may explain why the potential barrier increases on pressure, since a multiple inter-NGP tunneling is hindered by the multiple polymer separators that have to be penetrated quantum mechanically.

A straight line was fitted to the data points of PNC and PNC-PZ, respectively (Fig. 6). The slope equals the activation volume $v^{act} \cong \left(\frac{\partial E}{\partial P}\right)_T$ for each one of the relaxation mechanisms. The activation volume for DR1 is $2.6(6) \times 10^{-29} \text{ m}^3$ for PNC and $2.9(5) \times 10^{-29} \text{ m}^3$ for PNC-PZ, respectively. Within the experimental accuracy, we can conclude that the changes in the height of the potential barrier upon pressure of PNC and PNC-PZ is practically the same. This finding supports the scenario that the deformation and polarization procedure to render PNC to PNC-PZ does not affect DR1.

The dependence of the activation energy of DR2 upon pressure (Fig. 7) is quite different than of DR1. The deformation and polarization stages applied to PNC to render piezoelectric, yields to a systematic reduction of the potential barrier heights, apart from a singular behavior at 1250 bar, whereas PNC and PNC-PZ data points contribute to the appearance of a “spike”. DR2 is a high frequency dispersion, the relaxation time is shorter (compared with that of DR1) and, hence, the mean relaxation length. It is likely that DR2 stems from a single or few inter-NGP FIT. The differences observed between the effective potential barriers (and their dependencies on pressure) of PNC and PNC-PZ can be understood as follows: On increasing pressure, the corresponding activation energies evolve differently. The heterogeneity of both PNC and PNC-PZ is mainly characterized by the occurrence of sharp hard NGP flakes in a soft polymer blend matrix. Due to that a of heterogeneity, the external hydrostatic pressure results in an inhomogeneous internal stress field, whereas stress is locally amplified. In PNC, small scale relaxation is disturbed by the spatial fluctuation of the internal stress field. Hydrostatic compression of PNC-PZ yields an additional effect: piezoelectric PVdF grains are mechanically stimulated by those NGPs which are randomly in direct contact with PVdF and couple local electric fields. Fluctuations, due to heterogeneity, of the internal stress field and fluctuations, due to the piezo active PVdF, of the internal electric field couple to the temporal scale of charge transport process. Fluctuations affect rather a short-range electron transfer phenomenon (interfacial polarization DR2), rather than their macroscopic charge transport (such as dc conductivity).

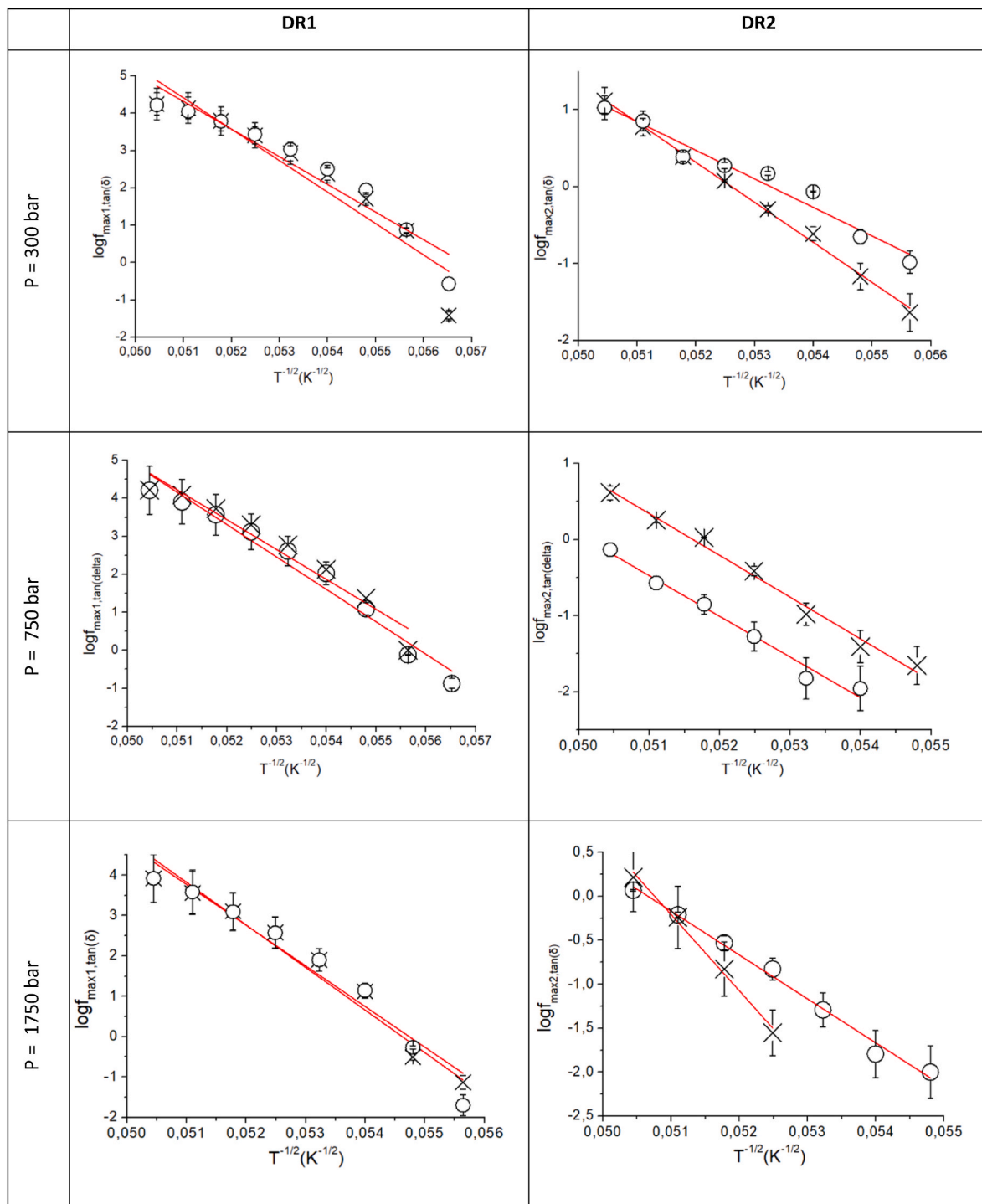


Fig. 5. Typical isobaric $\log f_{\max, \tan \delta}(T^{-1/2})$ diagrams. Straight lines are fitted to the data points, according to the FIT model. (o) : PNC, (x) : PNC-PZ). A comparative three dimensional representation is provided in the bottom graph.

5. Conclusions

Polymer Nanocomposites (PNC) of PVA/PVDF blends filled with NGPs, which render piezoelectric (PNC-PZ), were studied at various temperature and pressure conditions by using BDS. Dc electrical conductivity mechanisms are resolved by using the complex electric modulus formalism. Charge transport proceeds by (either single or multi-stage) -NGP fluctuation induced tunneling (FIT) of electrons through the effective potential barrier set by the polymer separating

neighboring NGPs, operate in successive temperature regions. The glass transition temperature and the temperature where the kinetics of water molecules bound to PVA gain increased mobility were earlier detected by DSC. Their shift toward higher temperature on increasing pressure, is realized by their signatures to the electric modulus spectrum. The estimated activation energy and activation volume for individual dc conductivity mechanism, profile their changes upon the alteration of the rubber state of the polymer blend and onset of the increased mobility of bound water molecules. Comparing the results for PNC and PNC-PZ, we

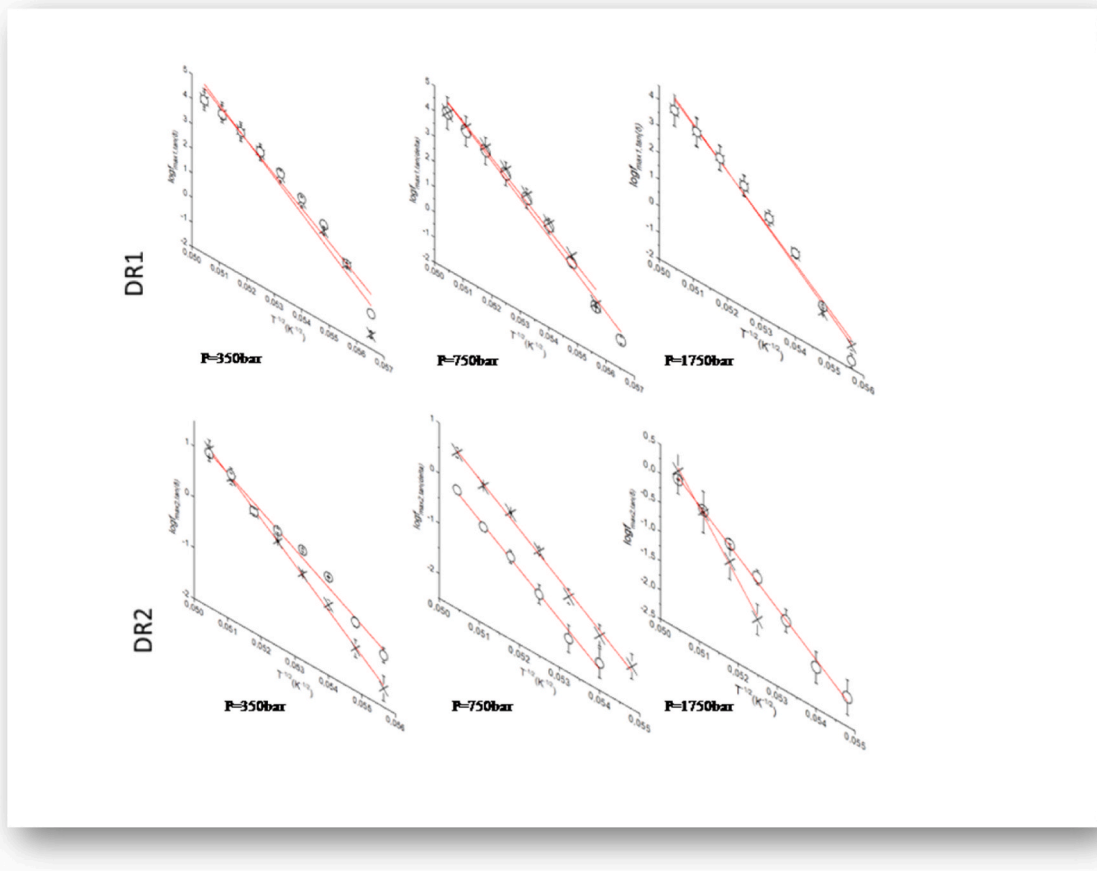


Fig. 5. (continued).

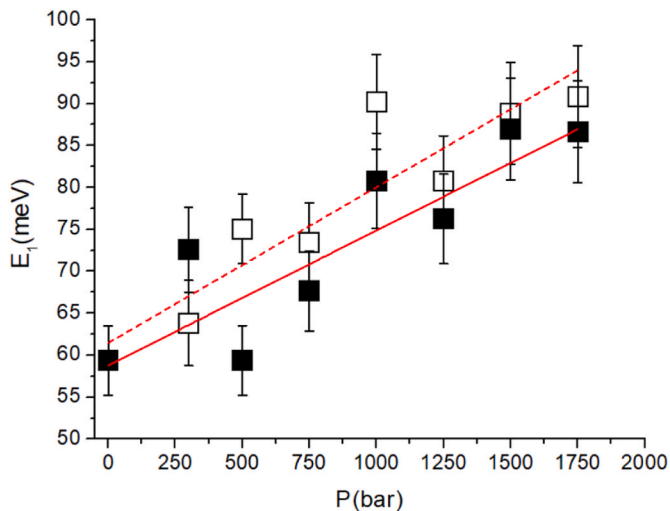


Fig. 6. The activation energy for relaxation mechanism DR1. Open squares correspond to fresh PNCs and full squares to the piezo-electric one, respectively.

found that the conduction mechanisms are not practically affected by the normal or piezoelectric state of the PVdF micro-grains. The evolutions of microstructure and crystalline phases under varying pressure are crucial for understanding the dielectric properties of the composites, would be a challenge for further exploration.

The dispersion of NGPs results in the appearance of two dielectric relaxation peaks in the tangent of the loss angle formalism. The low frequency mechanism involves relaxation of electrons within large

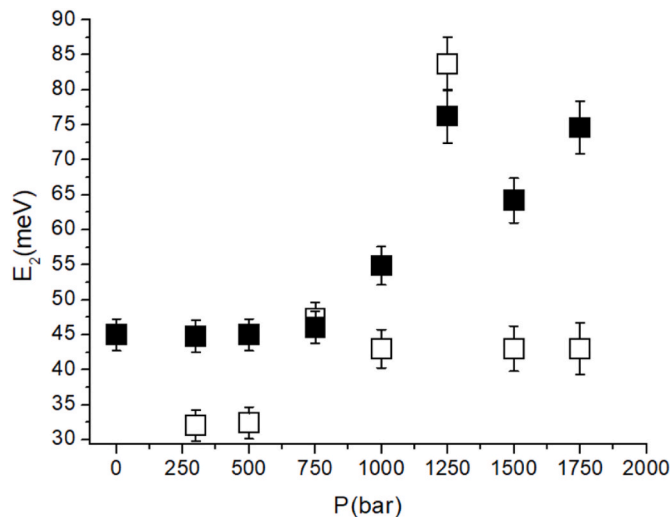


Fig. 7. The activation energy for relaxation mechanism DR1. Open squares correspond to fresh PNCs and full squares to the piezo-electric ones.

localization clusters over a large number of inter-NGP transitions. Activation energies and activation volumes are practically indistinguishable between PNC and PNC-PZ. The activation energy of a high frequency relaxation, which involves relaxation of trapped electrons within small sized regions, differs between PNC and PNC-PZ. On increasing pressure, the corresponding activation energies evolve differently. The heterogeneity of both PNC and PNC-PZ is mainly characterized by the occurrence of sharp hard NGP flakes in a soft

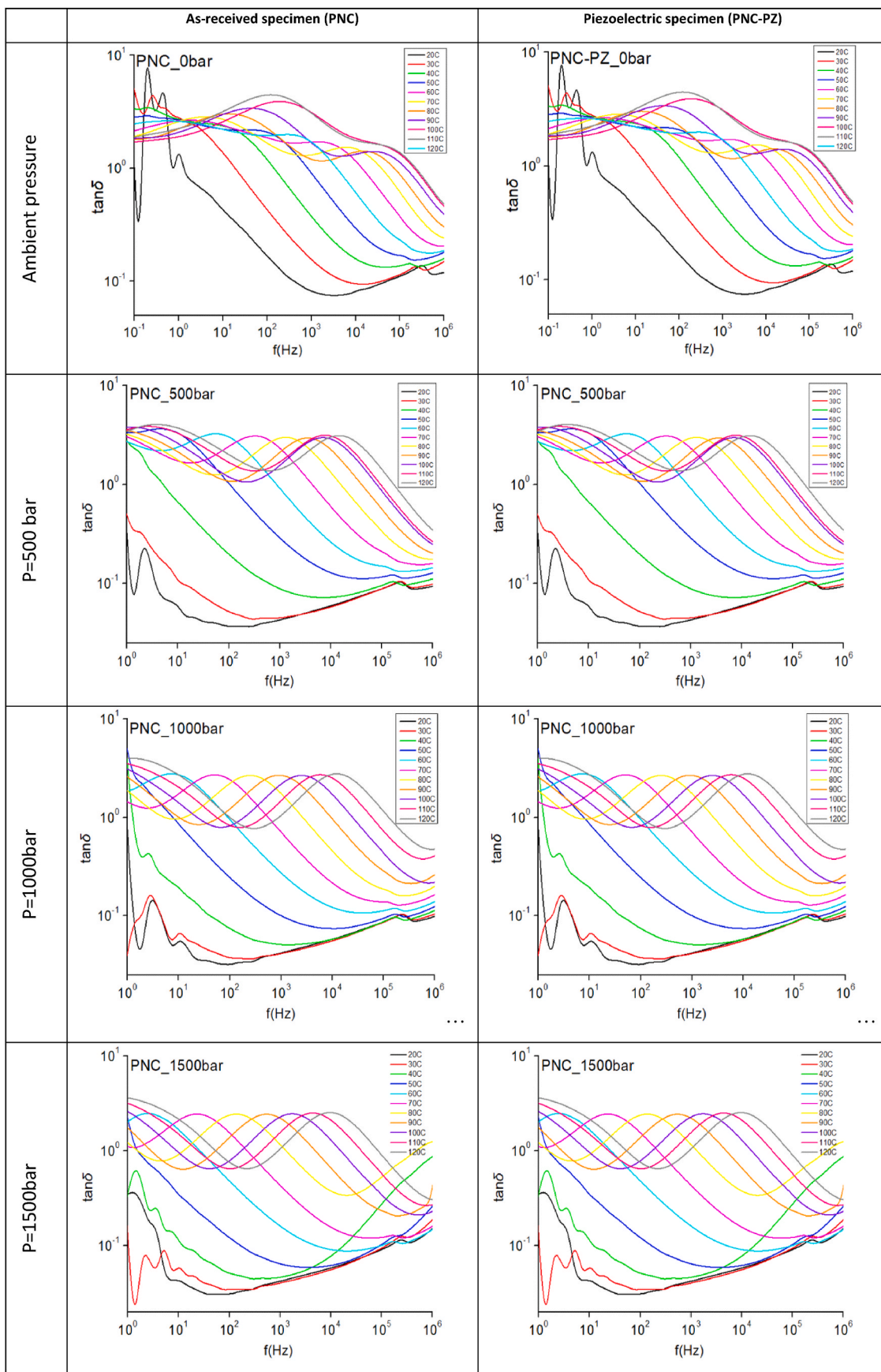


Fig. 8. $\tan\delta(f)$ isotherms for four different pressures sampled from the entire set of isobars recorded.

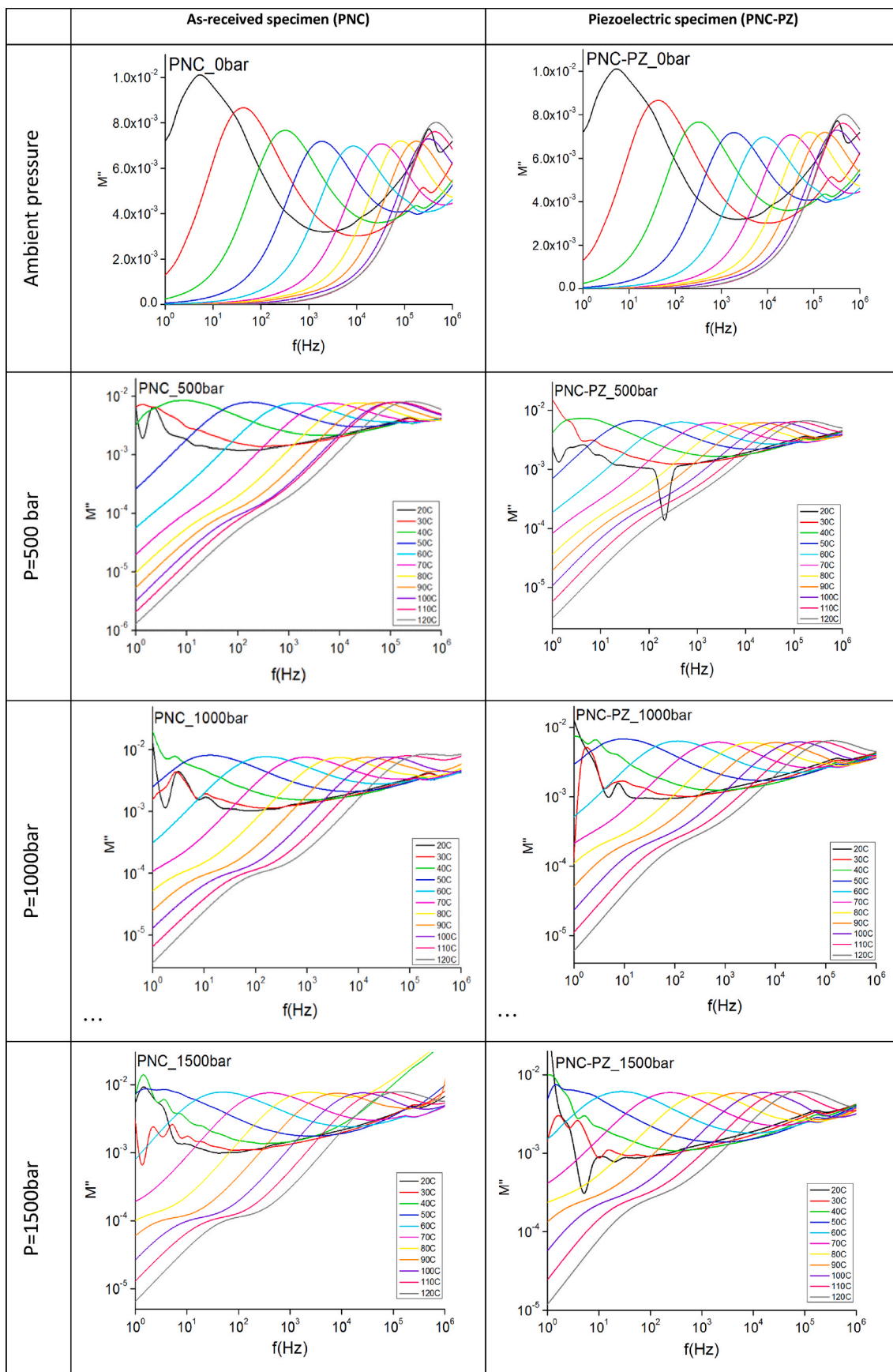


Fig. 9. Isotherms of $M''(f)$ spectra at representative pressures for PNC and PNC-PZ.

polymer blend matrix. Due to that heterogeneity, the external hydrostatic pressure results in an inhomogeneous internal stress field, whereas stress is locally amplified. In PNC, small scale relaxation is disturbed by the spatial fluctuation of the internal stress field. Hydrostatic compression of PNC-PZ yields an additional effect: piezoelectric PVDF grains are mechanically stimulated by those NGPs which are randomly in direct contact with PVDF and couple local electric fields. Regarding the role of heterogeneity and piezo activity, we may conclude that fluctuations (of the internal stress or electric field) affect rather a short-range electron transfer phenomenon (interfacial polarization DR2), rather than their macroscopic charge transport (such as dc conductivity).

Ethical declaration

The authors declare that they have no conflict of interest.

Author statement

We disclose any financial and personal relationships with other people or organizations that could inappropriately influence (bias) our work. The work described has neither been published previously nor under evaluation in other journal. All authors contributed equally to this work. E. Kolonelou is the main investigator and A. N. Papathanassiou is the Project administrator.

Declaration of competing interest

The authors declare that they have no known competing financial interests or personal relationships that could have appeared to influence the work reported in this paper.

Data availability

Data will be made available on request.

References

- [1] M.G. Broadhurst, G.T. Davis, J.E. McKinney, R.E. Collins, Piezoelectricity and pyroelectricity in polyvinylidene fluoride—A model, *J. Appl. Phys.* 49 (1978) 4992.
- [2] D.K. Das-Gupta, On the nature of pyroelectricity in polyvinylidene fluoride, *Ferroelectrics* 33 (1981) 75.
- [3] G.R. Harris, R.C. Preston, A.S. DeReggi, The impact of piezoelectric PVDF on medical ultrasound exposure measurements, standards, and regulations, *IEEE Trans. Ultrason. Ferroelectrics Freq. Control* 47 (6) (2000) 1321.
- [4] F. Stuart Foster, K.A. Harasiewicz, M.D. Sherar, A history of medical and biological imaging with polyvinylidene fluoride (PVDF) transducers, *IEEE Trans. Ultrason. Ferroelectrics Freq. Control* 47 (6) (2000) 1363.
- [5] W.P. Mason, Technical digests: an electromechanical representation of a piezoelectric crystal used as a transducer, *Bell System Technical Journal* 14 (4) (1935) 718.
- [6] E. Kolonelou, E. Loupou, P.A. Klonos, Sakellis Elias, D. Valadorou, A. Kyritsis b, A. N. Papathanassiou, Thermal and electrical characterization of poly(vinylalcohol)/poly(vinylidene fluoride) blends reinforced with nano-graphene platelets, *Polymer* (2021), <https://doi.org/10.1016/j.polymer.2021.123731>.
- [7] Ch Lampadaris, I. Sakellis, A.N. Papathanassiou, Dynamics of electric charge transport and determination of the percolation insulator-to-metal transition in polyvinylpyrrolidone/nano-graphene platelet composites, *Appl. Phys. Lett.* 110 (2017), 222901, <https://doi.org/10.1063/1.4984203>.
- [8] Eirini Kolonelou, Anthony N. Papathanassiou, Sakellis Elias, Evidence of Local Softening in Glassy Poly(vinyl Alcohol)/poly(vinyl Pyrrolidone) (1/1, W/w) Nano-Graphene Platelets Composites Materials Chemistry and Physics, 2018, <https://doi.org/10.1016/j.matchemphys.2018.10.058>.
- [9] Esmaeel Azadian, et al., Polyvinyl alcohol modified polyvinylidene fluoride-graphene oxide scaffold promotes osteogenic differentiation potential of human induced pluripotent stem cells, *J. Cell. Biochem.* 121 (2020) 3185–3196, 5-6.
- [10] Hojin Kim, Anabel Renteria-Marquez, Md Didarul Islam, Luis A. Chavez, Carlos A. Garcia Rosales, Md Ariful Ahsan, Tzu-Liang Bill Tseng, Norman D. Love, Yirong, Fabrication of bulk piezoelectric and dielectric BaTiO₃ ceramics using paste extrusion 3D printing technique, *LinFirst published: 04 December*, <https://doi.org/10.1111/jace.16242>, 2018.
- [11] G. Krishna Bama, Indra Devi, Ramachandran Structural and thermal properties of PVdF/PVA blends, *J. Mater. Sci.* 44 (2009) 1302–1307, <https://doi.org/10.1007/s10853-009-3271-8>.
- [12] P. Sheng, J. Klafter, Hopping conductivity in granular disordered systems, *Phys. Rev. B* 27 (4) (1983) 2583–2586.
- [13] P. Pissis, A. Kyritsis, Hydration studies in polymer hydrogels, *J. Polym. Sci. B Polym. Phys.* 51 (2013) 159–175.
- [14] A. Wurm, M. Ismail, B. Kretzschmar, D. Pospiech, C. Schick, Retarded crystallization in polyamide/layered silicates nano-composites caused by an immobilized interphase, *Macromolecules* 43 (2010) 1480–1487.
- [15] R. Bosio, C. Gorini, G. Fleury, J.-L. Pichard, Gate-modulated thermopower of disordered nanowires: II. Variable-range hopping regime, *New J. Phys.* 16 (2014), <https://doi.org/10.1088/1367-2630/16/9/095005>. Article ID 095005.
- [16] A.N. Papathanassiou, O. Mykhailiv, L. Echevoyen, I. Sakellis, M. Plonska-Brzezinska, Electric properties of carbon nano-onion/polyaniline composites: a combined electric modulus and ac conductivity study, *J. Phys. D Appl. Phys.* 48 (2016), 285305.
- [17] P.S. Das, P.K. Chakraborty, B. Behera, R.N.P. Choudhary, Electrical properties of Li₂BiV₅O₁₅ ceramics, *Phys. B Condens. Matter* 395 (2007) 98–103. <https://doi.org/10.1016/j.physb.2007.02.065>.
- [18] Belfiore, *Physical Properties of Macromolecules*, 2010, p. 177.
- [19] Eirini Kolonelou, Anthony N. Papathanassiou, Sakellis Elias, Pressure-induced Electro-Switching of Polymer/nano-Graphene Composites Materials Chemistry and Physics, 2019, pp. 319–324, <https://doi.org/10.1016/j.matchemphys.2019.05.002>.
- [20] S.B. Aziz, M.H. Hamsan, M.F.Z. Kadir, H.J. Woo, Design of polymerblends based on chitosan:POZ with improved dielectric constant for application in polymer electrolytes and flexible electronics, *Adv. Polym. Technol.* 2020 (2020), 8586136, <https://doi.org/10.1155/2020/8586136>.
- [21] H. Manjunatha, R. Damle, K. Pravin, G.N. Kumaraswamy, Modification in the transport and morphological properties of solid polymer electrolyte system by low-energy ionirradiation, *Ionics* 24 (2018) 3027–3037, <https://doi.org/10.1007/s11581-018-2518-2>.
- [22] H.J. Woo, S.R. Majid, A.K. Arof, Dielectric properties and morphology of polymer electrolyte based on poly(caprolactone) and ammonium thiocyanate, *Mater. Chem. Phys.* 134 (2012) 755–761, <https://doi.org/10.1016/j.matchemphys.2012.03.064>.
- [23] M. Ravi, Y. Pavani, K. Kiran Kumar, S. Bhavani, A.K. Sharma, V.V.R. Narasimha Rao, Studies on electrical and dielectric properties of PVP:KBrO₄ complexed polymer electrolyte films, *Mater. Chem. Phys.* 130 (2011) 442–448, <https://doi.org/10.1016/j.matchemphys.2011.07.006>.